3. Kadosh, D. & Struhl, K. Repression by Ume6 involves recruitment of a complex containing Sin3 corepressor and Rpd3 histone deacetylase to target promoters. *Cell* **89,** 365–371 (1997).
4. Nagy, L. *et al*. Nuclear receptor repression mediated by a complex containing SMRT, mSin3A, and histone deacetylase *Cell* **89,** 373–380 (1997).
5. Heinzel, T. *et al*. A complex containing N-CoR, mSin3 and histone deacetylase mediates transcriptional repression. *Nature* **387,** 43–48 (1997).
6. Alland, L. *et al*. Role for N-CoR and histone deacetylase in Sin3-mediated transcriptional repression. *Nature* **387,** 49–55 (1997).
7. Rundlett, S. E. *et al*. HDA1 and RPD3 are members of distinct yeast histone deacetylase complexes that regulate silencing and transcription. *Proc. Natl Acad. Sci. USA* **93,** 14503–14508 (1996).
8. Slekar, K. H. & Henry, S. A. SIN3 works through two different promoter elements to regulate INO1 gene expression in yeast. *Nucleic Acids Res.* **23,** 1964–1969 (1995).
9. Strich, R. *et al*. UME5 is a key regulator of nitrogen repression and meiotic development. *Genes Dev.* **8,** 796–810 (1994).
10. Hecht, A., Strahl-Bolsinger, S. & Grunstein, M. Spreading of transcriptional repressor SIR3 from telomeric heterochromatin. *Nature* **383,** 92–96 (1996).
11. Kasten, M. M., Dorland, S. & Stillman, D. J. A large protein complex containing the yeast Sin3p and Rpd3p transcriptional regulators. *Mol. Cell. Biol.* **17,** 4852–4858 (1997).
12. Zhang, Y. *et al*. Histone deacetylases and Sap18, a novel polypeptide, are components of a human Sin3 complex. *Cell* **89,** 357–364 (1997).
13. Mitchell, A. P. Control of meiotic gene expression in *Saccharomyces cerevisiae*. *Microbiol. Rev.* **58,** 56–70 (1964).
14. Grunstein, M. Histone function in transcription. *Annu. Rev. Cell Biol.* **6,** 643–678 (1990).
15. Luger, K., Mader, A. W., Richmond, R. K., Sargent, D. F. & Richmond, T. J. Crystal structure of the nucleosome core particle at 2.8 Å resolution. *Nature* **389,** 251–260 (1997).
16. Dean-Johnson, M. & Henry, S. A. Biosynthesis of inositol in yeast. Primary structure of myo-inositol-1-phosphate synthase (EC5.5.1.4) and functional analysis of its structural gene, the INO1 locus. *J. Biol. Chem.* **264,** 1274–1283 (1989).
17. Mann, R. K. & Grunstein, M. Histone H3 N-terminal mutations allow hyperactivation of the yeast GAL1 gene *in vivo*. *EMBO J.* **11,** 3297–3306 (1992).
18. Guthrie, C. & Fink, G. R. *Guide to Yeast Genetics and Molecular Biology* (Academic, San Deigo, CA, 1991).
19. Kayne, P. S. *et al*. Extremely conserved histone H4 N terminus is dispensable for growth but essential for repressing the silent mating loci in yeast. *Cell* **55,** 27–39 (1988).
20. Laman, H., Balderes, D. & Shore, D. Disturbance of normal cell cycle progression enhances the establishment of transcriptional silencing in *Saccharomyces cerevisiae*. *Mol. Cell. Biol.* **15,** 3608–3617 (1995).
21. Flomerfelt, F. A., Briehl, M. M., Dowd, D. R., Dieken, E. S. & Miesfeld, R. L. Elevated glutathione S-transferase gene expression is an early event during steroid-induced lymphocyte apoptosis. *J. Cell. Physiol.* **154,** 573–581 (1993).
22. Strahl-Bolsinger, S., Hecht, A., Luo, K. & Grunstein, M. SIR2 and SIR4 interactions differ in core and extended telomeric heterochromatin in yeast. *Genes Dev.* **11,** 83–93 (1997).
23. Clarke, D. J., O'Neill, L. P. & Turner, B. Selective use of H4 acetylation sites in the yeast *Saccharomyces cerevisiae*. *Biochem. J.* **294,** 557–561 (1993).
24. Vidal, M., Strich, R., Esposito, R. E. & Gaber, R. F. RPD1 (SIN3/UME4) is required for maximal activation and repression of diverse yeast genes. *Mol. Cell. Biol.* **11,** 6306–6316 (1991).

Acknowledgements. We thank S. Henry for discussions and R. Gaber for plasmid pMV117. This work was supported by Public Health Service grants from the NIH (to M.G.).

Correspondence and requests for materials should be addressed to M.G. (e-mail: mg@mbi.ucla.edu).

Structure of the calcium pump from sarcoplasmic reticulum at 8-Å resolution

Peijun Zhang*, Chikashi Toyoshima†, Koji Yonekura†‡, N. Michael Green§ & David L. Stokes*

** Skirball Institute of Biomolecular Medicine, New York University Medical Center, 540 First Avenue, New York, New York 10016, USA*
† Institute of Molecular and Cellular Biosciences, The University of Tokyo, Bunkyo-ku, Tokyo 113, Japan
§ National Institute for Medical Research, The Ridgeway, Mill Hill, London NW7 1AA, UK

The calcium pump from sarcoplasmic reticulum (Ca^{2+}-ATPase) is typical of the large family of P-type cation pumps. These couple ATP hydrolysis with cation transport, generating cation gradients across membranes. Ca^{2+}-ATPase specifically maintains the low cytoplasmic calcium concentration of resting muscle by pumping calcium into the sarcoplasmic reticulum; subsequent release is used to initiate contraction. No high-resolution structure of a P-type pump has yet been determined, although a 14-Å structure of Ca^{2+}-ATPase, obtained by electron microscopy of frozen-hydrated, tubular crystals[1], showed a large cytoplasmic head connected to the transmembrane domain by a narrow stalk. We have now improved the resolution to 8 Å and can discern ten transmembrane α-helices, four of which continue into the stalk. On the basis of constraints from transmembrane topology, site-directed mutagenesis and disulphide crosslinking, we have made tentative assignments for these α-helices within the amino-acid sequence. A distinct cavity leads to the putative calcium-binding site, providing a plausible path for calcium release to the lumen of the sarcoplasmic reticulum.

As in previous studies[2–4], tubular crystals were induced in rabbit sarcoplasmic reticulum by using decavanadate. We also included an inhibitor, dansyl thapsigargin[5], that promotes crystallization by

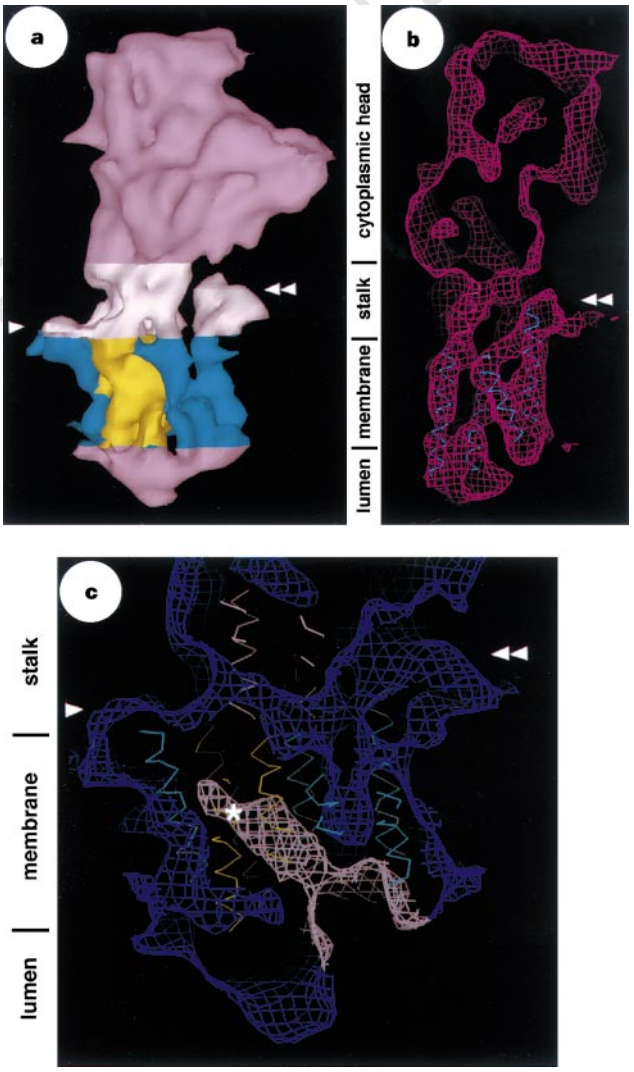

Figure 1 Ca^{2+}-ATPase density map at 8-Å resolution. **a**, Surface representation of the whole molecule with the raised platform (double arrowhead) and flat platform (single arrowhead) indicated. The cyan and yellow densities in the transmembrane domain correspond to the α-helices in **b**, **c** and Fig. 3. **b**, View of helices G, H, I and J (blue) fitted to the map; the 'tenth', highly inclined helix (I) is second from the left, and the helical hairpin composed by G and H is on the right. This view is rotated 90° relative to that in **a**, looking from the right at the model in **a**. **c**, A cavity within the transmembrane domain has been highlighted in grey and leads to putative calcium sites (asterisk). This contour level accounts for 100% of the molecular volume (147,000 $Å^3$ based on a relative molecular mass of 110,000), whereas contour levels in **a** and **b** correspond to 75% of this volume. The view is the same as that in **a**, but only a section from the centre of the molecule is shown, to reveal the cavity. The lines composing the nets in **b** and **c** are at 2-Å intervals.

‡ Present address: Protonic Nanomachine Project, ERATO, JST, 3-4 Hikaridai, Seika, 619-02 Kyoto, Japan.

locking Ca^{2+}-ATPase in the so-called E_2 conformation, which is characterized by low-affinity calcium binding from the lumenal side of the membrane[6]. Tubes were imaged in the frozen-hydrated state, and optical diffraction of the best images revealed a strong layer line at 10.5-Å resolution. The narrowest tubes (600 Å in diameter) were selected for image processing, which involved a combination of Fourier space averaging and real-space averaging (see Methods). The phase residuals indicated that the resulting data extended to at least 8-Å resolution (Table 1).

The resulting map (Figs 1, 2) reveals many rod-like densities, separated by ~10 Å, that presumably correspond to α-helices. Because the transmembrane and stalk domains are predicted to be entirely α-helical (Fig. 3), we have concentrated exclusively on these regions. Initially, α-carbon backbones were easily fitted to nine rod-like densities within the transmembrane domain (Fig. 2c–f), but this left a strong, unmatched density on the lumenal side of the membrane (arbitrarily labelled 'I' in Fig. 2f). Given the strong consensus for ten transmembrane helices[7–9], a tenth, highly inclined

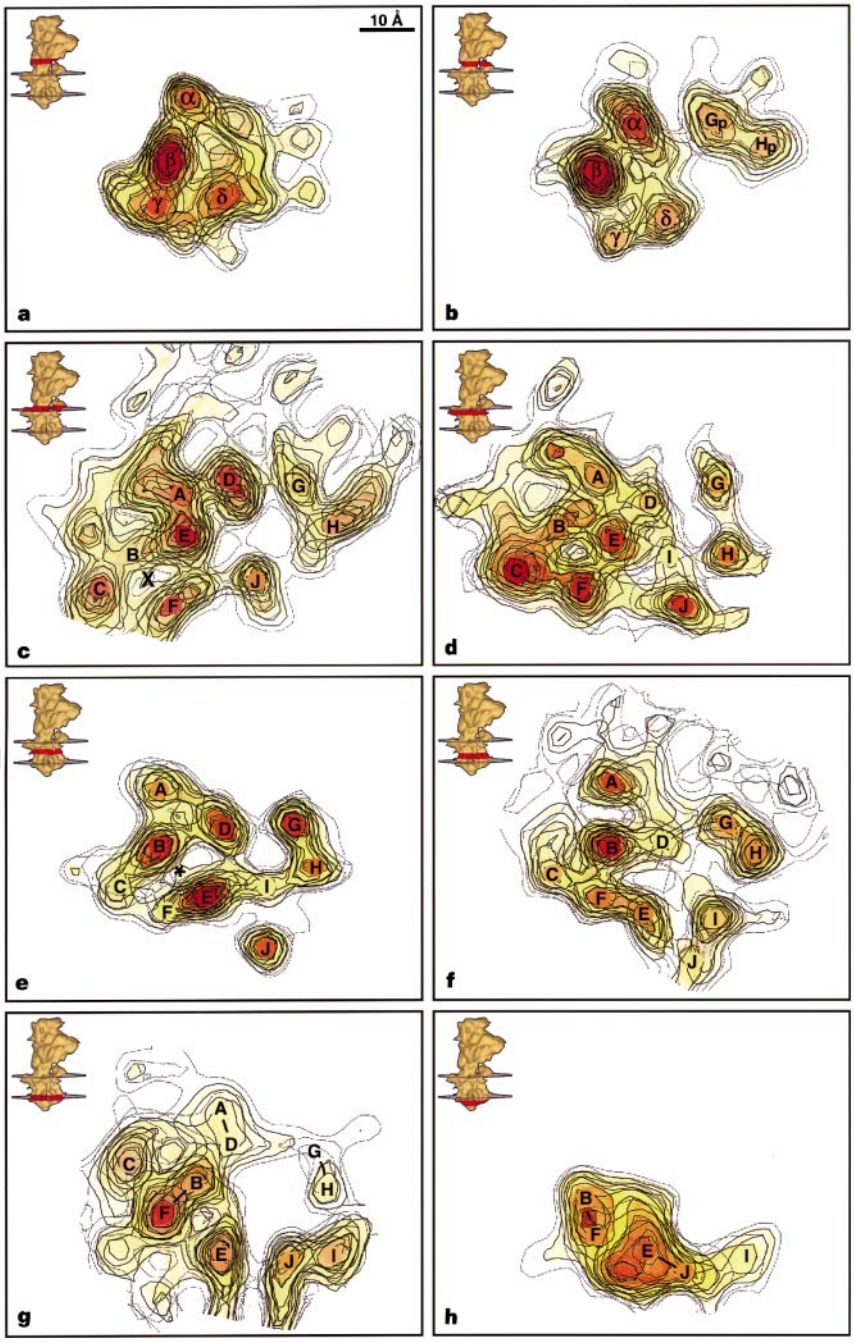

Figure 2 Density cross-sections through the transmembrane and stalk of Ca^{2+}-ATPase. Four sections (2 Å thick) were superimposed in each panel (**a**–**h**) and their position is shown on the inset surface model. The top of the cavity is marked by an asterisk in **e** at the same location as in Fig. 1c. The narrow passageway from the cytoplasm is marked with a cross in **c**. The lowest, dotted contour corresponds to 100% volume recovery; yellow, orange and red indicate increasing density.

Table 1 Statistics of data averaging

	$n_{1,0}$, $n_{0,1}$*			Real-space average	Edited average†
	–21,6	–22,6	–23,6		
No. of tubes	6	10	7	23	23
No. of molecules	16,368	22,976	12,400	51,744	51,744
Unit cell dimension					
a (Å)	57.1 ± 0.6	57.6 ± 0.2	57.9 ± 0.5		
b (Å)	116.6 ± 0.6	116.4 ± 1.7	115.8 ± 1.2		
γ (°)	63.9 ± 0.6	64.8 ± 0.5	65.2 ± 0.5		
Twofold phase residual (°)‡					
20.0 Å	7.4	5.9	8.7	3.1	3.1 (96)
14.4 Å	34.9	27.6	33.4	18.0	17.5 (91)
10.0 Å	42.3	38.9	43.1	31.9	29.6 (79)
8.0 Å	44.9	44.0	45.1	42.2	34.6 (57)

* Selection rule of the three independent data sets is characterized by the Bessel order (*n*) of the (1,0) and the (0,1) layer lines as defined in ref. 1.
† This data set, used for the final map, included 183 layer lines and was truncated at 8-Å resolution. It was derived from the real-space average by limiting the radial extent of each layer line to exclude noisy data with poor twofold phase residuals. Numbers in parentheses indicate the percentage of data remaining after editing. Overall phase residual was 16.2°.
‡ Amplitude-weighted phase residuals for twofold symmetry excluded equatorial data as well as data lower than 0.1% of the maximal off-equatorial amplitude (~99% of off-equatorial data were included). Random phases produce a phase residual of 45°.

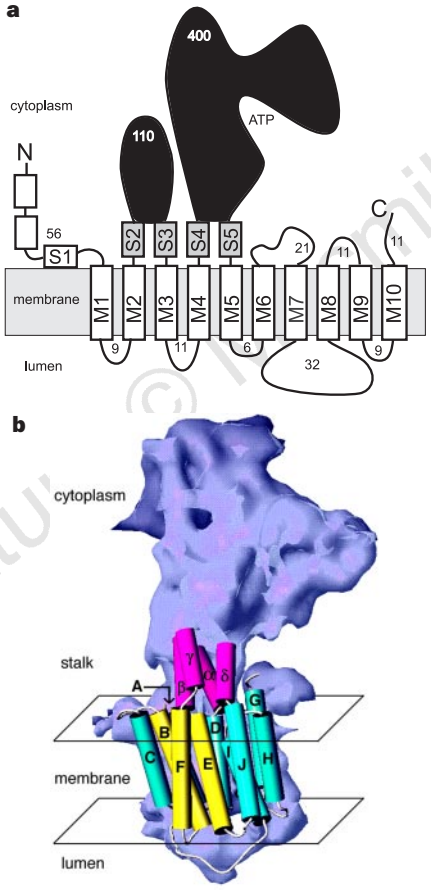

Figure 3 Transmembrane architecture of Ca^{2+}-ATPase. **a**, Rectangles correspond to predicted α-helices and numbers indicate the number of residues in intervening loops. Stalk helices are grey and exclude S1, given that only four stalk segments are observed in our map. The two long black loops compose the cytoplasmic domains, which carry out ATP hydrolysis, but were not fitted. **b**, The result of fitting transmembrane and stalk helices to our density map. An important feature is the three-stranded coiled coil formed by the yellow helices, which give rise to the cavity seen in Fig. 1c as helices E and I diverge toward the lumenal surface. All fitted helices were straight, although at higher resolution some might turn out to be bent. The white loops give a sense of continuity between helices based on the sequence assignments in Fig. 5a, but are not of accurate length.

helix was fitted to this last density. Unlike the initial nine helices, helix I does not traverse the membrane fully but meets helix E 6–8 Å from the cytoplasmic surface of the membrane (Fig. 2c, d). In general, only two of the ten helices (D and F) are inclined by <10°, five helices by 18° to 22°, and helices E and I by 27° and 34°, respectively, causing the relative positions of helices to change dramatically in sections parallel to the membrane plane (Fig. 2). Nevertheless, there are several clear groupings and a general trend toward right-handed twisting in these groups. In particular, pairwise associations occur between helices G and H, as well as between I and J, with the latter pair twisting around one another with a right-handed sense. A right-handed twist is seen again in the looser association between helices A and D and in the three-way association between helices B, E and F; at the cytoplasmic surface of the membrane, helix C is also associated with the latter group, but is excluded towards the lumenal membrane surface. Between this threesome is a cavity (asterisk in Figs 1c, 2e) leading from the middle of the membrane to the lumenal surface that is visible even at a contour level that includes 100% of the expected molecular volume (Fig. 1c) and appears to be surrounded exclusively by protein as it traverses the hydrophobic core of the bilayer. The presence of such a cavity is consistent with a water-filled channel that could provide access from the calcium-binding sites to the lumen, as would be expected for the E_2 conformation believed to populate this crystal form[4]. Such a channel has previously been hypothesized to explain voltage effects on sodium binding to the E_2 conformation of the related Na^+/K^+-ATPase[10,11], which suggest that cations move more than halfway across the membrane to reach their binding sites. Cytoplasmic access to the calcium sites should be restricted in the E_2 conformation, but even so there is a potential passageway starting at the cytoplasmic surface between helices B, C, E and F (cross in Fig. 2c) and leading down to the beginning of the larger cavity (asterisk in Fig. 2e). This passage is visible only at a higher density cutoff, which is consistent with the restricted access expected for cytoplasmic calcium in the E_2 conformation.

The stalk is 24 Å long and divided into four, rod-like densities, labelled α, β, γ and δ (Fig. 2b). The connection between these stalk densities and the transmembrane helices is obscured by the low contrast around the phosphate headgroups of the lipid bilayer (Fig. 2c). Nevertheless, the trajectory of α, β and δ densities suggest that they connect with transmembrane helices D, E and J, respectively; β and δ are almost collinear with E and J, whereas α is inclined at ~40° relative to D. According to structure predictions[7] (Fig. 3a), the stalk is composed of four or five α-helices, and we found that α-helical backbones fit plausibly into α, β and δ densities. However, the fourth stalk density, γ, is smaller, has lower density throughout the stalk and a tenuous connection with transmembrane helix F; thus the identification of γ as a stalk helix and its association with F remains tentative. Densities G_p and H_p (Fig. 2b) form a raised platform on the cytoplasmic surface of the membrane directly above helices G and H; as seen in Fig. 1 (double arrowhead), these densities are set apart from the stalk and do not connect with the main cytoplasmic head, and so are less likely to connect transmembrane sequences with either of the two, large cytoplasmic loops (Fig. 3). A second, flat platform caps transmembrane helices A, B and C at the cytoplasmic membrane surface to the left of the stalk (single arrowhead in Fig. 1). On the lumenal side of the membrane, a small, compact domain bridges helices I and J to a larger group containing helices B, C, E and F (Figs 1a and 2g, h). Helices G and H come together at the lumenal surface and have only weak associations with surrounding densities, and so resemble a helical hairpin (Fig. 1b).

We then tried to associate transmembrane and stalk densities with helices predicted from the amino-acid sequence (Fig. 3). These predictions[7] are supported by the current evidence for transmembrane topology[8,12] and provide two important constraints in the form of direct connections between stalk helices and particular

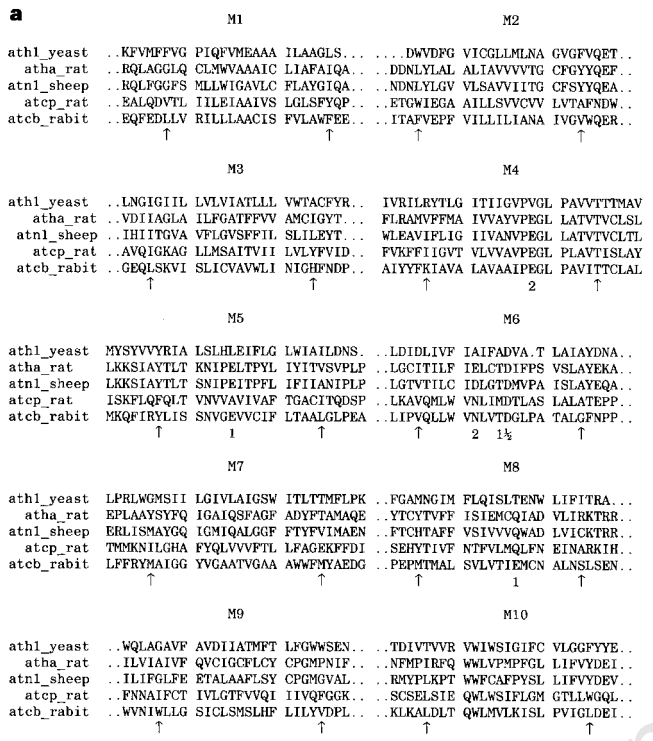

Figure 4 Variability within the transmembrane sequences of P-type ion pumps. **a**, Sequence alignment between representatives of several subfamilies of P-type pumps: from the top, yeast H^+-ATPase, rat H^+/K^+-ATPase, sheep Na^+/K^+-ATPase, rat plasma-membrane Ca^{2+}-ATPase and rabbit sarcoplasmic-reticulum Ca^{2+}-ATPase. These alignments were done according to refs 19, 25, but M8 for the PMCA and Na^+/K^+ families were realigned to match Q with E 908 from SERCA1[26]. Arrows define residues plotted in **b**; 1 and 2 indicate residues that contribute to calcium sites I and II[9], respectively. **b**, Residue conservation was analysed within three subfamilies[19] and variable residues are indicated by encircled letters for SERCA pumps, by filled circles for PMCA pumps, and by filled triangles for the Na^+/K^+-ATPase pumps. The helical wheels were superimposed on the density map (Fig. 2e) according to our most favoured assignment (Fig. 5a), and are oriented to expose variable faces to the lipid[18] and to juxtapose calcium ligands[13] (letters in triangles) and cysteine crosslinks[17] in M4, M5 and M6. Letters correspond to the sequence of SERCA1; helices with normal letters are running away from, and those with mirrored letters towards the cytoplasm. The first residue in each helix is numbered at the centre and marked with a filled diamond; the first heptad along the helix is numbered (2–7) and linked to corresponding residues in successive heptads by the curved arrows.

transmembrane helices, and close proximity between several pairs of transmembrane helices connected by short loops. Further constraints come from the results of site-directed mutagenesis, which localized the calcium-binding sites between M4, M5 and M6 (refs 9, 13–16), and from disulphide links between pairs of cysteines introduced into M4 and M6 (ref. 17). The positions of the linked cysteines support a right-handed coiling of M4 and M6 over several helical turns. Residue variability can also shed light on helix packing, given the tendency for variable sites to face the lipid and for conserved sites to participate in helix–helix interactions[18]. We have extended a previous analysis[19] by aligning transmembrane segments from several families of P-type pumps (Fig. 4a), using a few well-conserved markers within, or just outside, the hydrophobic segments and assuming an absence of gaps. The variable sites (Fig. 4b) of Na^+/K^+-ATPases (triangles) and plasma-membrane Ca^{2+}-ATPases (circles) correspond well with those of SR Ca^{2+}-ATPases (encircled letters), supporting the existence of a common transmembrane structure for the three families, even though there is less than 20% identity between the sequences of the transmembrane segments. In terms of helix packing, M4 and M6 are clearly the most highly conserved helices and should therefore have minimal exposure to bulk lipid. M5 is slightly less conserved, followed by M1, M2 and M8. M3, M9 and M10 are highly variable and the variable residues fall on one side of these helices, defining a face likely to be exposed to lipid. The specific positions of helices in Fig. 4b correspond to a section through the middle of the membrane at

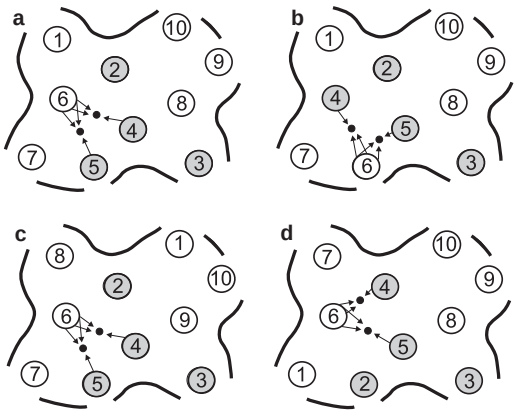

Figure 5 Alternative sequence assignments for the transmembrane helices. Although we favour the assignments in **a**, the ambiguity in the connection between stalk and transmembrane helices could produce assignments like that in **b**, in which the cavity would still be surrounded by M4, M5 and M6. A more direct assignment of the N terminus to the raised platform is shown in **c**, but the long distance between M8 and M9 is inconsistent with their short connecting loop; also, the corresponding M9–M10 loop is inconsistent with the map. The assignments in **d**, suffer from the higher exposure of M4 to the lipid and from the large distance between M4 and M6 at the cytoplasmic side of the membrane, where disulphide crosslinking was most efficient[17]. M2, M3, M4 and M5 have been shaded to reflect their predicted connection to stalk helices. The small filled black circles correspond to the two bound calcium ions, and arrows emanate from residues thought to coordinate these ions (see Fig. 4b).

the level expected for calcium-binding sites (~12 Å from the cytoplasmic surface; Fig. 2e); although the relative positions of helices change through the membrane, the exposed faces are generally preserved (Fig. 2).

Unfortunately, these constraints and considerations are not sufficient to assign unambiguously the sequence of transmembrane helices in our map. Nevertheless, we favour one set of assignments (Figs. 4b and 5a) over several others (Fig. 5b–d), which together provide specific hypotheses to be tested by further mutagenesis and crosslinking studies. Our preference is based on the most likely connections between stalk helices and transmembrane helices, for example $\alpha \rightarrow D$, $\beta \rightarrow E$, $\gamma \rightarrow F$ and $\delta \rightarrow J$ (Fig. 3b). The connection between γ and F is the most tenuous and, if correct, would probably involve an unstructured region near the membrane surface. Transmembrane density E is most central and so has been associated with the most highly conserved, stalk-associated helix, M4. Densities B, E and F form a right-handed coiled-coil that surrounds the distinctive cavity, and have thus been assigned to M4, M5 and M6. The geometry of this arrangement (Fig. 4b) is consistent with the mutagenesis results that associate particular residues with either of the two calcium-binding sites and specifically place them side by side at the intersection of channels from the cytoplasmic and lumenal sides of the membrane[9]. Assignment of M8 to the highly inclined density I allows E908 to project into the latter channel, consistent with its effects on calcium transport[9,13,14]; M8 would thus be rather short, perhaps owing to the unwinding of its polar carboxy terminus (NSLSEN; Fig. 4a). Density J is very exposed to lipid yet clearly extends into the stalk, making it a good candidate for the variable M3 helix. The extreme variability of M9 and M10 make this helical hairpin an attractive candidate for the isolated pair of transmembrane densities G and H, which are clearly associated at the lumenal side of the membrane (Fig. 1b). Indeed, these assignments are consistent with the lumenal disposition of several transmembrane densities (Fig. 2f–h), although the visualization of short loops at this resolution may in itself be unreliable. The loop between M7 and M8 is the longest, composing the bulk of the lumenal domain and presenting an exposed, antigenic site[20,21], consistent with M7 and M8 being on opposite sides of the molecule. An apparent discrepancy arises from putting the larger amino terminus in the flat platform and the smaller C terminus in the raised platform. This could be explained either by a disordered N terminus, or by putting the N terminus in the raised platform and hypothesizing a disordered or unstructured connection to M1; in the latter case, the arch of density connecting G with A in Fig. 2c could represent this connection.

Thus, we have resolved ten helices within the transmembrane domain of Ca^{2+}-ATPase and tentatively identified the site of calcium binding. Consistent with the conformation in this crystal form, a large cavity provides access to this site from the lumen, with a constricted passageway leading to the cytoplasmic surface. This suggests an oblique overall path for calcium through the molecule, and structural studies of the alternative E_1 conformation will be required to define the structural changes that drive transport along this path. □

Methods

Crystals were prepared as described[1], except that 30 μM dansyl thapsigargin[5] was added during crystallization. New strategies were used for processing images. To begin, a reference data set was compiled from the two best images in each of three symmetry groups ($n = 6$ for (0,1) layer line and $n = -21, -22$ or -23 for (1,0) layer lines according to previous nomenclature[1]) using established methods. Individual tubes were divided into short stretches (~1,000 Å) and positional parameters refined by comparing Fourier data with data from the corresponding reference data set[22]. This procedure corrected slight stretching and bending of the tubes, led to improved phase statistics over previous methods, and allowed the use of longer areas along slightly bent tubes, improving signal-to-noise ratios significantly. Initial defocus levels were determined from Fourier amplitudes obtained either from nearby carbon film or from the tube itself[23], and were later refined by comparing phases from the individual tubes with those in the averaged data sets. Data from each symmetry group were averaged and compensated for the contrast transfer function assuming 4.6% amplitude contrast[24]. These three independent averaged data sets were edited to exclude noisy data, and were truncated at either 14- or 10-Å resolution before calculating three-dimensional maps. After adjusting their relative magnifications, molecules within the three unit cells were masked and aligned in real space by cross-correlation; at this stage, twofold symmetry was not enforced and alignment parameters were determined independently for the twofold related molecules composing the unit cell. New maps were then created from a full set of unedited data to 6.5-Å resolution, aligned according to these same alignment parameters, weighted according to the square root of the number of contributing molecules, and averaged in real space (Table 1). This averaged map was then used to generate a set of Fourier data with the helical symmetry of the alignment reference ($n = -22$ for (1,0) layer line), which were edited and truncated to 8-Å resolution before calculating the final map.

Received 3 December 1997; accepted 20 January 1998.

1. Toyoshima, C., Sasabe, H. & Stokes, D. L. Three-dimensional cryo-electron microscopy of the calcium ion pump in the sarcoplasmic reticulum membrane. *Nature* **362,** 469–471 (1993).
2. Dux, L. & Martonosi, A. Two-dimensional arrays of proteins in sarcoplasmic reticulum and purified Ca^{2+}-ATPase vesicles treated with vanadate. *J. Biol. Chem.* **258,** 2599–2603 (1983).
3. Taylor, K. A., Dux, L. & Martonosi, A. Three-dimensional reconstruction of negatively stained crystals of the Ca^{++}-ATPase from muscle sarcoplasmic reticulum. *J. Mol. Biol.* **187,** 417–427 (1986).
4. Stokes, D. L. & Lacapere, J.-J. Conformation of Ca^{2+}-ATPase in two crystal forms: Effects of Ca^{2+}, thapsigargin, AMP-PCP, and Cr-ATP on crystallization. *J. Biol. Chem.* **269,** 11606–11613 (1994).
5. Hua, S., Malak, H., Lakowicz, J. R. & Inesi, G. Synthesis and interaction of fluorescent thapsigargin derivatives with the carcoplasmic reticulum ATPase membrane-bound region. *Biochemistry* **34,** 5137–5142 (1995).
6. Sagara, Y., Wade, J. B. & Inesi, G. A conformational mechanism for formation of a dead-end complex by the sarcoplasmic reticulum ATPase with thapsigargin. *J. Biol. Chem.* **267,** 1286–1292 (1992).
7. MacLennan, D. H., Brandl, C. J., Korczak, B. & Green, N. M. Amino-acid sequence of a $Ca^{2+} + Mg^{2+}$-dependent ATPase from rabbit muscle sarcoplasmic reticulum, deduced from its complementary DNA sequence. *Nature* **316,** 696–700 (1985).
8. Moller, J. V., Juul, B. & le Maire, M. Structural organization, ion transport, and energy transduction of ATPases. *Biochim. Biophys. Acta* **1286,** 1–51 (1996).
9. MacLennan, D. H., Rice, W. J. & Green, N. M. The mechanism of Ca^{2+} transport by sarco(endo)-plasmic reticulum Ca^{2+} ATPases. *J. Biol. Chem.* **272,** 28815–28818 (1997).
10. Gadsby, D. C., Rakowski, R. F. & De Weer, P. Extracellular access to the Na, K pump: Pathway similar to ion channel. *Science* **260,** 100–103 (1993).
11. Hilgemann, D. W. Channel-like function of the Na,K pump probed at microsecond resolution in giant membrane patches. *Science* **263,** 1429–1432 (1994).
12. Stokes, D. L., Taylor, W. R. & Green, N. M. Structure, transmembrane topology and helix packing of P-type ion pumps. *FEBS Lett.* **346,** 32–38 (1994).
13. Clarke, D. M., Loo, T. W., Inesi, G. & MacLennan, D. H. Location of high affinity Ca^{2+}-binding sites within the predicted transmembrane domain of the sarcoplasmic reticulum Ca^{2+}-ATPase. *Nature* **339,** 476–478 (1989).
14. Andersen, J. P. Dissection of the functional domains of the sarcoplasmic reticulum Ca^{2+}-ATPase by site-directed mutagenesis. *Biosci. Rep.* **15,** 243–261 (1995).
15. Rice, W. J. & MacLennan, D. H. Scanning mutagenesis reveals a similar pattern of mutation sensitivity in transmembrane sequences M4, M5, and M6, but not in M8, of the Ca^{2+}-ATPase of sarcoplasmic reticulum (SERCA1a). *J. Biol. Chem.* **271,** 31412–31419 (1996).
16. Chen, L. *et al.* Short and long range functions of amino acids in the transmembrane region of the sarcoplasmic reticulum ATPase: a mutational study. *J. Biol. Chem.* **271,** 10745–10752 (1996).
17. Rice, W. J. & MacLennan, D. H. Site-directed disulfide mapping of helices M4 and M6 in the Ca^{2+} binding domain of SERCA1a, the Ca^{2+} ATPase of fast-twitch skeletal muscle sarcoplasmic reticulum. *J. Biol. Chem.* **272,** 31412–31419 (1997).
18. Baldwin, J. M. The probable arrangement of the helices in G protein-coupled receptors. *EMBO J.* **12,** 1693–1703 (1993).
19. Green, N. M. in *The Sodium Pump: Structure, Mechanisms, Hormonal Control and its Role in Disease* (eds Bamberg, E. & Schoner, W.) 110–119 (Steinkopff, Darmstadt, 1994).
20. Matthews, I., Sharma, R. P., Lee, A. G. & East, J. M. Transmembranous organization of (Ca^{2+}-Mg^{2+})-ATPase from sarcoplasmic reticulum: evidence for lumenal location of residues 877–888. *J. Biol. Chem.* **265,** 18737–18740 (1990).
21. Clarke, D. M., Loo, T. W. & MacLennan, D. H. The epitope for monoclonal antibody A20 (amino acids 870–890) is located on the luminal surface of the Ca^{2+}-ATPase of sarcoplasmic reticulum. *J. Biol. Chem.* **265,** 17405–17408 (1990).
22. Beroukhim, R. & Unwin, N. Distortion correction of tubular crystals: Improvements in the acetylcholine receptor structure. *Ultramicroscopy* **70,** 57–81 (1997).
23. Tani, K., Sasabe, H. & Toyoshima, C. A set of computer programs for determining defocus and astigmatism in electron images. *Ultramicroscopy* **65,** 31–44 (1997).
24. Toyoshima, C., Yonekura, K. & Sasabe, H. Contrast transfer for frozen-hydrated specimens: II. Amplitude contrast at very low frequencies. *Ultramicroscopy* **48,** 165–176 (1993).
25. Green, N. M. ATP-driven cation pumps: alignment of sequences. *Biochem. Soc. Trans.* **17,** 970–972 (1989).
26. Guerini, D., Foletti, D., Vellani, F. & Carofoli, E. Mutation of conserved residues in transmembrane domains 4, 6, and 8 causes loss of Ca^{2+} transport by the plasma membrane Ca^{2+} pump. *Biochemistry* **35,** 3290–3296 (1996).

Acknowledgements. We thank R. Beroukhim and N. Unwin for the use of their programs for helical image analysis, and G. Inesi for the dansyl thapsigargin. This work was partly supported by the NIH and the Ministry of Education, Science, Sports and Culture of Japan.

Correspondence and requests for materials should be addressed to D.L.S. (e-mail: stokes@saturn.med.nyu.edu).